Low-temperature electronic properties of Sr_2RuO_4. I. Microscopic model and normal-state properties

Ralph Werner* and V. J. Emery†
Physics Department, Brookhaven National Laboratory, Upton, New York 11973-5000
(Received 11 March 2002; revised manuscript received 20 August 2002; published 9 January 2003)

Starting from the quasi-one-dimensional kinetic energy of the d_{yz} and d_{zx} bands we derive a bosonized description of the correlated electron system in Sr_2RuO_4. At intermediate coupling the magnetic correlations have a quasi-one-dimensional component along the diagonals of the basal plane of the tetragonal unit cell that accounts for the observed neutron scattering results. Together with two-dimensional correlations the model consistently accounts for the normal phase specific heat, cyclotron mass enhancement, static susceptibility, and Wilson ratio and implies an anomalous high-temperature resistivity.

DOI: 10.1103/PhysRevB.67.014504 PACS number(s): 74.70.−b, 71.10.−w, 71.45.−d, 75.45.+j

I. INTRODUCTION

Sr_2RuO_4 is the first layered transition metal oxide that exhibits superconductivity in the absence of copper ions.[1] The lattice symmetry is tetragonal and isostructural to La_2CuO_4 with lattice parameters $a=b=3.87$ Å in the RuO_2 plane and $c=12.74$ Å out-of-plane. No structural instabilities are observed.[2] The first de Haas–van Alphen (dHvA) results[3] and band structure calculations in local density approximation (LDA)[4] show three bands cutting the Fermi level with quasi two-dimensional Fermi surfaces. They can be mainly associated with the three t_{2g} orbitals of the Ru^{4+} ions,[5,6] and are consistent with the metallic properties and the strongly anisotropic transport along the c axis.[1]

The enhanced specific heat and magnetic susceptibility indicate the presence of significant correlations.[1] Consistently, results from angle resolved photoemission spectroscopy (ARPES)[7] and dHvA measurements[3] suggest a strong electronic mass renormalization. The material is Fermi liquid like in a temperature range of $T_c<T<30$ K.[8–10]

The significant correlations in Sr_2RuO_4, the $S=1$ moments on Ru^{4+} impurities in Sr_2IrO_4,[11] and ferromagnetic correlations in $SrRuO_3$ led Rice and Sigrist[12] to propose that the superconducting order parameter has p-wave symmetry promoted by ferromagnetic correlations analogous to ^{3}He. The absence of a change in the Knight shift in the superconducting phase[13,14] supported that notion as well as the temperature independent magnetic susceptibility[15] and the enhanced relaxation time in Muon spin resonance (μSR)[16] at $T\leqslant T_c\sim 1.5$ K. A similar proposal was made by Baskaran based on a comparison with high-T_c materials and emphasizing the role of Hund's rule coupling.[17]

Since then tremendous experimental effort has been made trying to verify the predicted p-wave symmetry of the superconducting order parameter. Neither tunneling[18,19] nor thermal conductivity experiments[20–22] or ac-susceptibility measurements[23] under different magnetic field geometries gave conclusive proof of the analogy to ^{3}He. No indication for ferromagnetic correlations has been found in ARPES,[24,25] LDA,[26,27] or neutron scattering[28,29] investigations. Furthermore, the specific heat[30–32] and nuclear quadrupole resonance[10] are consistent with two-dimensional gapless fluctuations in the superconducting phase of Sr_2RuO_4 which are absent in superfluid ^{3}He.

The controversy about the proper description of the electronic correlations in Sr_2RuO_4 is reflected most impressively by the variation of values of the on-site Coulomb repulsion U used in the mostly perturbative approaches to match experimental results. Examples are $U\approx 0.42$ eV,[33] 0.2 eV,[34] 1.2–1.5 eV,[35] 0.345 eV,[36,37] 0.175 eV,[38] 2 eV,[39] 0.048 eV.[40] Comparing these values of the interaction with the bare Fermi velocity of $\overline{v}_F\approx 0.7$ eVa from band-structure calculations[27] and ARPES[25] points toward an intermediate coupling regime.

In contrast to the effects of the interactions the bare electronic band structure has been determined unambiguously from dHvA,[41,42] ARPES,[24] and x-ray-absorption measurements[5] in consistency with LDA calculations.[27,33] The overlap of the electronic wave functions of the d_{zx} and d_{yz} orbitals is dominantly one dimensional.[6,27,33] The interaction and additional hopping channels lead the d_{zx} and d_{yz} electrons to hybridized into two bands. Their Fermi surfaces are referred to as the α and β sheets. The electrons in the d_{xy} orbital form the two-dimensional γ sheet.[27,33]

Correlations in effective one-dimensional systems show power-law behavior.[43] They are always more singular than two-dimensional correlations which diverge at most logarithmically.[44] Since the kinetic energy of the d_{zx} and d_{yz} electrons is quasi-one-dimensional we expect their correlations to play a dominant role.

The quasi-one-dimensional kinetic energy of the d_{zx} and d_{yz} electrons allows for the bosonized, nonperturbative description of the low-energy electronic excitations. This description is introduced in Sec. II and its fundamental properties are discussed. Section III is devoted to the expected corrections from hybridization effects and the γ sheet that have been neglected in the initial model. The comparison with experimental results in Sec. IV reveals the qualitative and quantitative consistency of the model within the framework of its applicability. A comparitive discussion of alter-

native perturbative approaches is included [Sec. IV B].

The present paper is part I of a series of three. Part II (Ref. 45) is devoted to the superconducting phase. The in-plane correlations are described via the model derived herein. The interplane pair-correlations are enhanced as a consequence of the body-centered crystal structure and can be treated mean-field like.

Part III (Ref. 46) consistently explains the experimentally observed unconventional transitions under magnetic fields based on the model derived here and in part II.

II. SUBSYSTEM OF D_{zx} AND D_{yz} BANDS

The band structure as determined from dHvA,[41] ARPES,[24] and *x*-ray-absorption measurements[5] as well as LDA calculations[33,27] together with the anticipated intermediate interactions suggest a three band Hubbard Hamiltonian as the generic model.

$$H=\sum_{\substack{\boldsymbol{l},\boldsymbol{l}'\\ \nu,\sigma}} t_{\boldsymbol{l},\boldsymbol{l}'}^{\nu,\nu'} c_{\boldsymbol{l},\nu,\sigma}c_{\boldsymbol{l}',\nu,\sigma}+\sum_{\substack{\boldsymbol{l},\nu,\sigma\\ \nu',\sigma'}} U_{\sigma,\sigma'}^{\nu,\nu'} n_{\boldsymbol{l},\nu,\sigma}n_{\boldsymbol{l},\nu',\sigma'}. \quad (1)$$

In this notation the electron creation and annihilation operators are $c_{\boldsymbol{l},\nu,\sigma}^{\dagger}$ and $c_{\boldsymbol{l},\nu,\sigma}$ for orbital ν with spin σ on site $\boldsymbol{l}$, $n_{\boldsymbol{l},\nu,\sigma}$ is the usual electronic density operator, $t_{\boldsymbol{l},\boldsymbol{l}'}^{\nu,\nu'}$ is the hopping matrix element between site $\boldsymbol{l}$ and $\boldsymbol{l}'$, and $U_{\sigma,\sigma'}^{\nu,\nu'}$ is the on-site Coulomb repulsion.

As discussed in the introduction we expect the interesting low-temperature physics to be dominated by the quasi-one-dimensional d_{zx} ($\nu=x$) and d_{yz} ($\nu=y$) bands. We retain here only the dominant hopping amplitudes $t_0=t_{\boldsymbol{l},\boldsymbol{l}+\hat{x}}^{x,x}=t_{\boldsymbol{l},\boldsymbol{l}+\hat{y}}^{y,y}$ and discuss effects from the hybridization of the bands later in Sec. III. The continuum representation is introduced via $c_{\boldsymbol{l},\nu,\sigma}\rightarrow\psi_{\nu,\sigma}(\boldsymbol{r})$ with $\rho_{\nu,\sigma}(\boldsymbol{r})=\psi_{\nu,\sigma}^{\dagger}(\boldsymbol{r})\psi_{\nu,\sigma}(\boldsymbol{r})$. The bands are linearized with Fermi velocity $v_{\mathrm{F}}\approx\sqrt{3}\,t_0$. Note that the "velocities" in the present paper define the kinetic energy scales, i.e., $v_{\mathrm{F}}=\overline{v}_{\mathrm{F}}/a$ ($\hbar\equiv 1$).

$$H_{2\mathrm{D}}=\lim_{\substack{a\rightarrow 0\\ L\rightarrow\infty}}\sum_{\nu,\sigma}\int_{-L}^{L}d^2r\Bigg[iv_{\mathrm{F}}\psi_{\nu,\sigma}^{\dagger}(\boldsymbol{r})\partial_{\nu}\psi_{\nu,\sigma}(\boldsymbol{r})+\frac{1}{4}\sum_{\nu',\sigma'}\rho_{\nu,\sigma}(\boldsymbol{r})(U_0\sigma_{\nu,\nu'}^{0}\sigma_{\sigma,\sigma'}^{x}+U_1\sigma_{\nu,\nu'}^{x}\sigma_{\sigma,\sigma'}^{x}+U_2\sigma_{\nu,\nu'}^{x}\sigma_{\sigma,\sigma'}^{0})\rho_{\nu',\sigma'}(\boldsymbol{r})\Bigg]. \quad (2)$$

Here $\sigma_{a,a'}^{x,y,z,0}$ denote the Pauli matrices with $\sigma_{a,a'}^{0}=(\sigma_{a,a'}^{z})^2$ and $2L=L_x=L_y$ is the linear dimension of the system. We limit the description here to the RuO_2 planes and generalize when necessary to a three-dimensional array of planes. The intra-orbital Coulomb repulsion is larger than the interorbital repulsion, i.e., $U_{\sigma\neq\sigma'}^{\nu=\nu'}=U_0>U_1=U_{\sigma\neq\sigma'}^{\nu\neq\nu'}$ and $U_0>U_2=U_{\sigma=\sigma'}^{\nu\neq\nu'}$.

Hund's rule coupling lowers the interorbital Coulomb repulsion for electrons in a spin-triplet configuration with respect to the spin singlets. The full treatment of the involved exchange interaction terms within the framework of the bosonization approach discussed in Sec. II A is rather involved and only possible in approximations. A qualitative study of the effect of Hund's rule coupling is possible by setting $U_1>U_2$ and neglecting the exchange terms. The expected corrections due to exchange and other terms are discussed closer in Sec. II C.

The Hamiltonian Eq. (2) is SU(2) invariant both in the spin sector and in the orbital sector yielding an effective $\mathrm{SU}(2)\otimes\mathrm{SU}(2)$ symmetry. The orbital degrees of freedom are sometimes referred to as electron flavors.[47,48]

A. Bosonization

In Eq. (2) the d_{zx} fields only have a kinetic energy contribution along the *x* direction while the d_{yz} fields only have a kinetic energy along *y*. We can thus switch to the chiral representation[49]

$$\psi_{\nu,\sigma}(\boldsymbol{r})=R_{\nu,\sigma}(\boldsymbol{r})e^{ik_{\mathrm{F}}r_{\nu}}+L_{\nu,\sigma}(\boldsymbol{r})e^{-ik_{\mathrm{F}}r_{\nu}} \quad (3)$$

for each orbital degree of freedom ν at each position $r_{\nu'\neq\nu}$ transverse to the propagation. The right ($R_{\nu,\sigma}$) and left ($L_{\nu,\sigma}$) moving fermions of each species can now be bosonized.[47,43]

$$R_{\nu,\sigma}(\boldsymbol{r})=\lim_{a\rightarrow 0}\frac{\eta_{\nu,\sigma}^{R}(r_{\nu'})}{\sqrt{2\pi a}}e^{-i\sqrt{\pi}[\theta_{\nu,\sigma}(\boldsymbol{r})+\phi_{\nu,\sigma}(\boldsymbol{r})]}, \quad (4)$$

$$L_{\nu,\sigma}(\boldsymbol{r})=\lim_{a\rightarrow 0}\frac{\eta_{\nu,\sigma}^{L}(r_{\nu'})}{\sqrt{2\pi a}}e^{-i\sqrt{\pi}[\theta_{\nu,\sigma}(\boldsymbol{r})-\phi_{\nu,\sigma}(\boldsymbol{r})]}. \quad (5)$$

Here $\phi_{\nu,\sigma}(\boldsymbol{r})$ are the Bose fields with their conjugate momenta $\Pi_{\nu,\sigma}(\boldsymbol{r})=\partial_{\nu}\theta_{\nu,\sigma}(\boldsymbol{r})$ which satisfy the commutation relation

$$[\phi_{\nu,\sigma}(\boldsymbol{r}),\Pi_{\nu',\sigma'}(\boldsymbol{r}')]=i\delta_{\nu,\nu'}\delta_{\sigma,\sigma'}\delta(\boldsymbol{r}-\boldsymbol{r}'). \quad (6)$$

The Klein factors[50] $\eta_{\nu,\sigma}(r_{\nu'})$ assure the proper commutation relation between the different fermion species, a is a short-range cutoff associated with the in-plane lattice constant. The bosonized Hamiltonian can be written as

$$H_{2D}=\lim_{\substack{a\to 0\\ L\to\infty}}\sum_{\sigma\neq\sigma'}\sum_{\nu\neq\nu'}\int_{-L}^{L}d^2r\Bigg[\frac{v_F}{2}[\Pi_{\nu,\sigma}^2+(\partial_\nu\phi_{\nu,\sigma})^2]+\frac{U_0}{4}\Bigg([\partial_\nu\phi_{\nu,\sigma}][\partial_\nu\phi_{\nu,\sigma'}]+\frac{\cos\sqrt{4\pi}(\phi_{\nu,\sigma}-\phi_{\nu,\sigma'})}{(2\pi a)^2}\Bigg)+\frac{U_1}{4}[\partial_\nu\phi_{\nu,\sigma}]$$
$$\times[\partial_{\nu'}\phi_{\nu',\sigma'}]+\frac{U_1}{4(2\pi a)^2}\{\cos[\sqrt{4\pi}(\phi_{\nu,\sigma}-\phi_{\nu',\sigma'})-2k_F(r_\nu-r_{\nu'})]+\cos[\sqrt{4\pi}(\phi_{\nu,\sigma}+\phi_{\nu',\sigma'})-2k_F(r_\nu+r_{\nu'})]\}$$
$$+\frac{U_2}{4}[\partial_\nu\phi_{\nu,\sigma}][\partial_{\nu'}\phi_{\nu',\sigma}]+\frac{U_2}{4(2\pi a)^2}\{\cos[\sqrt{4\pi}(\phi_{\nu,\sigma}-\phi_{\nu',\sigma})-2k_F(r_\nu-r_{\nu'})]$$
$$+\cos[\sqrt{4\pi}(\phi_{\nu,\sigma}+\phi_{\nu',\sigma})-2k_F(r_\nu+r_{\nu'})]\}\Bigg]. \tag{7}$$

The standard approach to separate spin and charge degrees of freedom in Eq. (7) is to introduce charge and magnetic fields for each flavor via

$$\varphi_{\nu,m}(\boldsymbol{r})=[\phi_{\nu,\uparrow}(\boldsymbol{r})-\phi_{\nu,\downarrow}(\boldsymbol{r})]/\sqrt{2}, \tag{8}$$

$$\varphi_{\nu,c}(\boldsymbol{r})=[\phi_{\nu,\uparrow}(\boldsymbol{r})+\phi_{\nu,\downarrow}(\boldsymbol{r})]/\sqrt{2}, \tag{9}$$

respectively. $\Pi_{\nu,m}$ and $\Pi_{\nu,c}$ are the corresponding conjugate momenta. The bilinear part of the Hamiltonian H_{2D} is composed of the charge and (magnetic) part

$$H_{c\,(m)}=\frac{1}{2}\sum_\nu\int d^2r\Bigg[v_F\Pi_{\nu,c\,(m)}^2+\sum_{\nu'}(\partial_\nu\varphi_{\nu,c\,(m)})V_{\nu,\nu'}^{(c\,(m))}(\partial_{\nu'}\varphi_{\nu',c\,(m)})\Bigg]. \tag{10}$$

The matrix elements for the charge (magnetic) part are given by $V_{x,x}^{[c(m)]}=V_{y,y}^{[c(m)]}=v_F+(-)U_0$ and $V_{x,y}^{[c(m)]}=V_{y,x}^{[c(m)]}=U_1+(-)U_2$. Equation (10) is the Hamiltonian of a crossed *sliding Luttinger liquid* studied in Refs. 51 and 52. The authors find no significant change in the decay of the low-energy correlations with respect to the one-dimensional case where $V_{x,y}^{[c(m)]}=0$. A perturbative treatment suggests that the inclusion of the interaction term in Eq. (7) leads to two-dimensional correlations which still decay algebraically.[51] In the absence of Hund's rule coupling, where $U_2=U_1$, the magnetic sector fields $\varphi_{x,m}$ and $\varphi_{y,m}$ are decoupled. Similar models are obtained for coupled Luttinger liquids.[53–55]

To study the qualitative properties of the model defined by Eq. (7) with parameters relevant for Sr_2RuO_4 it proves useful to use the symmetry of the orbital degrees of freedom. We introduce charge ($\mu=\rho$), spin ($\mu=$s), flavor ($\mu=$f), and spin-flavor ($\mu=$sf) fields via the canonical transformation

$$\phi_\mu(\boldsymbol{r})=\frac{1}{2}\sum_{\nu,\sigma}\sigma_{\nu,\nu}^a\sigma_{\sigma,\sigma}^b\phi_{\nu,\sigma}(\boldsymbol{r}), \tag{11}$$

$$\Pi_\mu(\boldsymbol{r})=\frac{1}{2}\sum_{\nu,\sigma}\sigma_{\nu,\nu}^a\sigma_{\sigma,\sigma}^b\Pi_{\nu,\sigma}(\boldsymbol{r}). \tag{12}$$

The matrices are $(a,b)=\{(0,0);(0,z);(z,0);(z,z)\}$ for $\mu=\{\rho;$s;f;sf$\}$, respectively. The fields $\phi_\mu(\boldsymbol{r})$ are identical to those of the resonant-level model used to describe the two-channel Kondo problem.[47] The fields are simple linear combinations of the charge and magnetic fields, e.g.,

$$\phi_s(\boldsymbol{r})=(\varphi_{x,m}+\varphi_{y,m})/\sqrt{2}, \tag{13}$$

$$\phi_{sf}(\boldsymbol{r})=(\varphi_{x,m}-\varphi_{y,m})/\sqrt{2}. \tag{14}$$

Note also that the charge and spin sector fields are symmetry related via the reflection $y\to -y\Rightarrow R_{y,\sigma}\leftrightarrow L_{y,\sigma}\Rightarrow\phi_f\leftrightarrow\phi_\rho$ and $\phi_s\leftrightarrow\phi_{sf}$.

The representation can be simplified by introducing the variables $\overline{x}=(1/\sqrt{2})(x+y)$ and $\overline{y}=(1/\sqrt{2})(x-y)$ with $\overline{\mathbf{r}}=(\overline{x},\overline{y})^\dagger$. The charge Hamiltonian in Eq. (10) becomes

$$H_c=\frac{1}{2}\int d^2\overline{r}\{v_F(\Pi_\rho^2+\Pi_f^2)+V_c[\partial_{\overline{x}}\phi_\rho+\partial_{\overline{y}}\phi_f]^2+\overline{V}_c[\partial_{\overline{y}}\phi_\rho+\partial_{\overline{x}}\phi_f]^2\}, \tag{15}$$

while the magnetic Hamiltonian is

$$H_m=\frac{1}{2}\int d^2\overline{r}\{v_F(\Pi_s^2+\Pi_{sf}^2)+V_m[\partial_{\overline{x}}\phi_s+\partial_{\overline{y}}\phi_{sf}]^2+\overline{V}_m[\partial_{\overline{y}}\phi_s+\partial_{\overline{x}}\phi_{sf}]^2\}. \tag{16}$$

The energies are

$$V_c=v_F+U_0+(U_1+U_2), \tag{17}$$

$$\overline{V}_c=v_F+U_0-(U_1+U_2), \tag{18}$$

$$V_m=v_F-U_0+(U_1-U_2), \tag{19}$$

$$\overline{V}_m=v_F-U_0-(U_1-U_2). \tag{20}$$

Applying Eqs. (11) and (12) the interaction term in the Hamiltonian Eq. (7) factorizes into contributions of the four spin, charge, flavor, and spin-flavor degrees of freedom.

$$H_{\rm int}=\frac{U_0}{(2\pi a)^2}\int d^2\bar{r}\cos\sqrt{4\pi}\phi_{\rm s}(\bar{\mathbf{r}})\cos\sqrt{4\pi}\phi_{\rm sf}(\bar{\mathbf{r}})$$
$$+\frac{1}{(2\pi a)^2}\int d^2\bar{r}\cos[\sqrt{4\pi}\phi_{\rm f}(\bar{\mathbf{r}})-2\sqrt{2}k_{\rm F}\bar{y}]$$
$$\times[U_1\cos\sqrt{4\pi}\phi_{\rm s}(\bar{\mathbf{r}})+U_2\cos\sqrt{4\pi}\phi_{\rm sf}(\bar{\mathbf{r}})]$$
$$+\frac{1}{(2\pi a)^2}\int d^2\bar{r}\cos[\sqrt{4\pi}\phi_{\rho}(\bar{\mathbf{r}})-2\sqrt{2}k_{\rm F}\bar{x}]$$
$$\times[U_2\cos\sqrt{4\pi}\phi_{\rm s}(\bar{\mathbf{r}})+U_1\cos\sqrt{4\pi}\phi_{\rm sf}(\bar{\mathbf{r}})]. \quad (21)$$

The limit $a\to 0$ and $L\to\infty$ is understood. The total Hamiltonian of the d_{zx}-d_{yz} subsystem is $H_{\rm 2D}=H_{\rm c}+H_{\rm m}+H_{\rm int}$.

No spin or charge density wave instabilities are observed in Sr_2RuO_4.[28] The values for the on-site Coulomb repulsions discussed in the literature[33–36,39,38,40] point toward an intermediate coupling regime if compared to the bare Fermi velocity of $v_{\rm F}\approx 0.7$ eV from band structure calculations.[27] For repulsive interactions the operators in Eq. (21) have been shown to be marginally irrelevant both in one and two dimensions.[43] The physical properties are therefore determined by $H_{\rm c}$ and $H_{\rm m}$ with quantitative corrections from $H_{\rm int}$. Corrections from hybridization terms not included in the bosonized model are discussed in Sec. III.

Note that Eqs. (15) through (21) are still explicitly invariant under the reflection $x\leftrightarrow y$ which is equivalent to $\bar{x}\to\bar{x}$, $\bar{y}\to-\bar{y}$, $\phi_{\rm f}\to-\phi_{\rm f}$, and $\phi_{\rm sf}\to-\phi_{\rm sf}$. The same applies for $y\to-y$ where $\bar{x}\leftrightarrow\bar{y}$, $R_{y,\sigma}\leftrightarrow L_{y,\sigma}$, $\phi_{\rm f}\leftrightarrow\phi_{\rho}$ and $\phi_{\rm s}\leftrightarrow\phi_{\rm sf}$.

B. Effective one-dimensional model

In the intermediate coupling regime the model defined by Eqs. (15) through (21) exhibits a number of singular points for $V_{\rm c(m)}=0$ or $\bar{V}_{\rm c(m)}=0$. For $U_0<v_{\rm F}$ and $U_0>U_1>U_2$ the relevant limit is $\bar{V}_{\rm m}\to 0$. Then the magnetic Hamiltonian Eq. (16) only has terms in $\partial_{\bar{x}}\phi_{\rm s}$ and $\partial_{\bar{y}}\phi_{\rm sf}$.

$$H_{\rm m}^{-}=\frac{1}{2}\int d^2\bar{r}\{v_{\rm F}(\Pi_{\rm s}^2+\Pi_{\rm sf}^2)+V_{\rm m}[\partial_{\bar{x}}\phi_{\rm s}+\partial_{\bar{y}}\phi_{\rm sf}]^2\}. \quad (22)$$

The representation of the spin and spin-flavor fields introduced in Sec. II A has the property that along $x=y$ one finds $\partial_{\bar{y}}\phi_{\rm s}=\partial_{\bar{x}}\phi_{\rm sf}=0$. This becomes obvious from Eqs. (13) and (14) together with the symmetry[56] implied relation $\partial_y\varphi_{y,{\rm m}}|_{x=y}=\partial_x\varphi_{\bar{x},{\rm m}}|_{x=\bar{y}}$. Thus, the fields $\phi_{\rm s}$ and $\phi_{\rm sf}$ indeed depend only on $\bar{y}$ and $\bar{x}$, respectively, as implied by Eq. (22) and $H_{\rm m}^{-}$ is effectively one dimensional. Since the spin and the spin-flavor channel are symmetry related the one-dimensional correlations in Eq. (22) can be effectively described by

$$H_{\rm eff}=\frac{v_{\rm eff}L}{2}\int d\bar{x}[K_{\rm eff}\Pi_{\rm eff}^2+K_{\rm eff}^{-1}(\partial_{\bar{x}}\phi_{\rm eff})^2]. \quad (23)$$

Note that the coupling term $(\partial_{\bar{x}}\phi_{\rm s})(\partial_{\bar{y}}\phi_{\rm sf})$ in Eq. (22) can be eliminated by a mean-field decoupling and subsequent sliding transformation.[55] This approximation is less severe than it may appear at first sight since along $x=y$ the $\bar{x}$ dependence of $\phi_{\rm sf}$ and the $\bar{y}$ dependence of $\phi_{\rm s}$ can be neglected. Consequently, along $x=y$, $(\partial_{\bar{x}}\phi_{\rm s})$ is just a y-independent constant with respect to $(\partial_{\bar{y}}\phi_{\rm sf})$ and vice versa.

The Luttinger liquid parameter $K_{\rm eff}$ and the velocity $v_{\rm eff}$ are effective parameters of the theory[57] but can be associated with

$$K_{\rm eff}^{-1}\sim\sqrt{V_{\rm m}/v_{\rm F}} \quad (24)$$

and

$$v_{\rm eff}\sim\sqrt{V_{\rm m}v_{\rm F}}. \quad (25)$$

The model Eq. (22) is explicitly invariant under the transformation $y\to-y$, where $\bar{x}\leftrightarrow\bar{y}$ and $\phi_{\rm s}\leftrightarrow\phi_{\rm sf}$. The effective one-dimensional model Eq. (23) describes the quasi-one-dimensional magnetic correlations along both in-plane diagonals of the tetragonal unit cell.

In realistic systems $\bar{V}_{\rm m}>0$ and the effective model is applicable only for sufficiently large temperatures $T>\bar{V}_{\rm m}$. A close discussion of the values appropriate for Sr_2RuO_4 is given in Sec. IV.

The total Hamiltonian of the low-energy in-plane d_{zx}-d_{yz} correlations is given by $H_{\rm 2D}=H_{\rm c}+H_{\rm eff}+H_{\rm int}$ in Eqs. (15), (23), and (21). The interaction term $H_{\rm int}$ can be neglected when appropriately rescaling the parameters $K_{\rm eff}\to K_{\rm eff}^{*}$, $V_{\rm c}\to V_{\rm c}^{*}$, and $\bar{V}_{\rm c}\to\bar{V}_{\rm c}^{*}$.

After eliminating the term $\sim(\partial_{\bar{x}}\phi_{\rm s})(\partial_{\bar{y}}\phi_{\rm sf})$ in Eq. (23) by a sliding transformation the magnetic Hamiltonian can be written as a superposition $H_{\rm m}\approx H_{\rm s}+H_{\rm sf}\approx H_{\rm eff}$, where $H_{\rm s}$ and $H_{\rm sf}$ are obtained from Eq. (23) by replacing (eff→s) and (eff→sf, $\bar{x}\to\bar{y}$), respectively. Note that here $v_{\rm s}=v_{\rm sf}=v_{\rm eff}/2$. In the case of SU(2) symmetry in the spin subspace the interaction term Eq. (21) yields a rescaled $K_{\mu}\to K_{\mu}^{*}=1$. In Ref. 45 it is suggested that the spins of the electrons in the d_{zx}–d_{yz} subsystem are in an easy-plane configuration which implies $K_{\rm s}^{*}<1$ and $K_{\rm sf}^{*}\leqslant 1$.

C. Comment on Hund's rule coupling

The treatment of the full SU(2) invariant Hund's rule coupling term[17] $J_{\rm H}\boldsymbol{S}_{\nu}\boldsymbol{S}_{\nu'\neq\nu}$ is difficult in the bosonized model. The presence of SU(2) symmetry breaking Dzyaloshinskii–Moriya interactions is obvious from the observed anisotropies of the static susceptibilities[8,13] and is consistent with the expected presence of spin-orbit coupling in the Ru 4*d* orbitals.[37,58,59] Additional corrections are expected from Kaplan–Shekhtman–Entin-Wohlman–Aharony terms.[60]

The crucial physical implication of Hund's rule coupling is that it couples the magnetic degrees of freedom of the different orbitals. The model introduced in Sec. II A incorporates this effect qualitatively as becomes apparent from Eq. (10). Notably is $V_{\rm m}\neq\bar{V}_{\rm m}$ only for $U_1\neq U_2$ and consequently can the quasi-one-dimensional model discussed in Sec. II B

only be found in the presence of Hund's rule coupling. The quantitative justification of the model is shown phenomenologically in Sec. IV and in Refs. 45 and 46.

Note that the estimated value for Hund's rule coupling[35] in Sr_2RuO_4 of $J_H \approx 0.2-0.4$ eV is larger than the estimate for the spin-orbit coupling[59] of $\lambda \approx 0.1$ eV. Consequently the effective model for the magnetic correlations derived here is applicable even in the presence corrections from spin-orbit coupling that lifts the degeneracy of the d_{zx} and d_{yz} orbitals because the larger Hund's rule coupling overcompensates the effect.

III. INTERPLANE COUPLING AND BAND HYBRIDIZATION

The model described in Sec. II has been based on the two d_{zx} and d_{yz} bands that are coupled via the on-site interaction only. In this section we discuss the d_{xy} band as well as the d_{zx}-d_{yz} interchain and hybridization terms which are expected to qualitatively change the low-temperature physics of the bosonized model. Here we discuss the magnitude of the terms and their expected impact. In Sec. IV we then discuss at what temperature which properties of Sr_2RuO_4 are determined by a certain subsystem.

The in-plane resistivity is two to three orders of magnitude smaller than that along the c axis.[8] Consistently the dispersion of the Fermi energy along c is about 1% of the in-plane dispersion as probed by dHvA measurements.[41] Band-structure calculations lead to an estimated interplane hopping of about 10% of the in-plane hopping.[33]

The appropriate interplane Hamiltonian with hopping amplitude $t_\perp$ is

$$H_\perp = t_\perp \sum_{\nu,\nu'=x,y} \sum_{\boldsymbol{l},\boldsymbol{l}',\sigma} c^\dagger_{\boldsymbol{l},\nu,\sigma} c_{\boldsymbol{l}',\nu,\sigma}, \tag{26}$$

with only nearest-neighbors $\boldsymbol{R}_{\boldsymbol{l}'} = \boldsymbol{R}_{\boldsymbol{l}} + \frac{1}{2}(\pm a, \pm a, \pm c)^\dagger$. The interplane hopping of the d_{xy} band is an order of magnitude smaller[41] as a consequence of the in-plane geometry of the d_{xy} orbitals[6] and can be neglected. Fourier transforming the Fermi operators via

$$c_{\boldsymbol{l},\nu,\sigma} = \frac{1}{\sqrt{N}} \sum_{\boldsymbol{k}} e^{i\boldsymbol{k}\boldsymbol{R}_{\boldsymbol{l}}} c_{\boldsymbol{k},\nu,\sigma} \tag{27}$$

leads to

$$H_\perp = 8t_\perp \sum_{\nu,\sigma,\boldsymbol{k}} \cos\frac{ak_x}{2}\cos\frac{ak_y}{2}\cos\frac{ck_z}{2} c^\dagger_{\boldsymbol{k},\nu,\sigma} c_{\boldsymbol{k},\nu,\sigma}. \tag{28}$$

The in-plane kinetic energies of the d_{zx} and d_{yz} electrons are

$$H_\nu = 2t_0 \sum_{\sigma,\boldsymbol{k}} \cos(ak_\nu) c^\dagger_{\boldsymbol{k},\nu,\sigma} c_{\boldsymbol{k},\nu,\sigma}. \tag{29}$$

The total Hamiltonian for the d_{zx} and d_{yz} electrons $H_x + H_y + H_\perp$ can readily be diagonalized and yields the dispersion for the α and β bands as

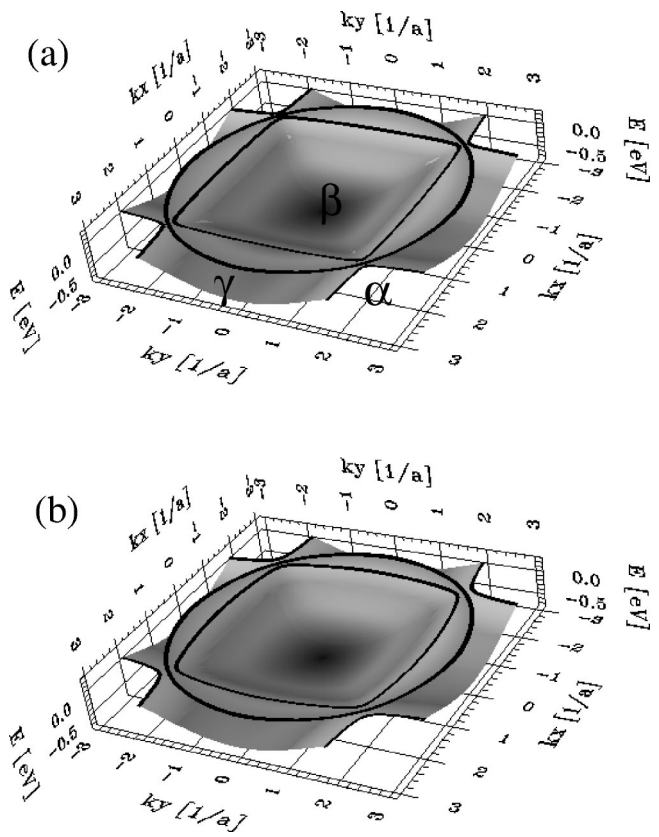

FIG. 1. Tight-binding model for the three bands that form the Fermi surface. (a) Reduced model with d_{zx}-d_{yz} hybridization trough interplane coupling Eq. (30). (b) Model including next-nearest-layer hopping, interchain coupling, and interaction induce on-site d_{zx}-d_{yz} hybridization Eq. (32) for $k_z = 0$.

$$E^{(\beta)}_{\boldsymbol{k}} = E_0 + t_0(\cos ak_x + \cos ak_y) + 8t_\perp g_{1,\boldsymbol{k}} \pm \frac{1}{2}\sqrt{t_0^2 g^2_{0,\boldsymbol{k}} + 256 t_\perp^2 g^2_{1,\boldsymbol{k}}}. \tag{30}$$

The abbreviations $g_{0,\boldsymbol{k}} = \cos(ak_x) - \cos(ak_y)$ and $g_{1,\boldsymbol{k}} = \cos(ak_x/2)\cos(ak_y/2)\cos(ck_z/2)$ were introduced for lucidity.

Panel (a) of Fig. 1 shows the resulting tight-binding bands for $k_z = 0$ as a function of k_x and k_y. The parameters are $E_0 = 0.22$ eV, $t_0 = -0.3$ eV, and $t_\perp = -0.02$ eV. The dispersion of the d_{xy} or γ band is given by

$$\frac{E^{(\gamma)}_{\boldsymbol{k}}}{\text{eV}} = -0.39 - 0.54(\cos ak_x + \cos ak_y) - 0.44 \cos ak_x \cos ak_y. \tag{31}$$

The term $\sim \cos ak_x \cos ak_y$ stems from in-plane next-nearest-neighbor hopping. The corresponding real-space hopping parameters are $t^{\gamma,\gamma}_{\boldsymbol{l},\boldsymbol{l}} = -0.39$ eV, $t^{\gamma,\gamma}_{\boldsymbol{l},\boldsymbol{l}+\hat{x}} = t^{\gamma,\gamma}_{\boldsymbol{l},\boldsymbol{l}+\hat{y}} = -0.27$ eV, and $t^{\gamma,\gamma}_{\boldsymbol{l},\boldsymbol{l}+\hat{x}+\hat{y}} = -0.11$ eV. The qualitative agreement with ARPES,[24] LDA,[33] and dHvA[3,6] results is satisfactory.

In order to obtain a more precise match with the three-dimensional Fermi surface suggested by dHvA

measurements[3,41] it is necessary to extend the dispersion for the α and β sheets in Eq. (30). The nonvanishing coefficient k_{02} in Ref. 41 suggest a term $2t_z\cos ck_z$ from next-nearest-layer hopping. Spin-orbit coupling in the d_{zx}-d_{yz} subsystem leads to a hybridization of the orbitals.[59,37] The fields in the Hamiltonians discussed in Sec. II A are describing hybridized d_{zx} and d_{yz} orbitals as a consequence of the on-site interaction.[61] In the framework of the tight-binding model these effects can be modeled by introducing the on-site hybridization t_h. The in-plane dispersion is also enhanced and can be modeled by extending the diagonal contributions Eq. (29) to include an effective interchain hopping $t_0\cos ak_\nu \rightarrow t_0\cos ak_\nu + t_i\cos ak_{\nu'\neq\nu}$. The resulting dispersions are

$$\tilde{E}^{(\alpha)}_{\boldsymbol{k}} = \tilde{E}_0 + (t_0+t_i)(\cos ak_x + \cos ak_y) + 2t_z\cos ck_z + 8t_\perp g_{1,\boldsymbol{k}} \pm \frac{1}{2}\sqrt{t_0^2 g_{0,\boldsymbol{k}}^2 + 256 t_\perp^2 g_{1,\boldsymbol{k}}^2 + 4t_h^2}. \tag{32}$$

An appropriate choice of parameters is $\tilde{E}_0 = -0.29$ eV, $t_0 = 0.3$ eV, $t_i = 0.03$ eV, $t_z = 0.02$ eV, $t_\perp = 0.02$ eV, and $t_h = 0.06$ eV. The resulting bands are shown in Fig. 1 panel (b) for $k_z = 0$.

The tight-binding analysis leads to the following conclusions:

(i) The two- and three-dimensional corrections to the quasi-one-dimensional d_{zx} and d_{yz} bands are of the order of 10% or 0.03 eV leading to the presence of the α and β sheets of the Fermi surface. Luttinger liquid behavior should only be observable at sufficiently high-temperatures. For $T > t_{i,z,\perp,h} \sim 400$ K the out-of-plane transport is incoherent and saturates while the in-plane resistivity is determined by the crossed sliding Luttinger liquid with linear temperature dependence. Consequently the model is consistent with the observed anomalous high-temperature resistivity.[62] Also consistent is that the quasi-particle peaks observed in ARPES disappear above $T \sim 160$ K.[63,64]

(ii) Since the on-site interactions are an order of magnitude larger than the tight-binding parameters, i.e., $U_{0,1,2} \gg t_{i,h,\perp,z}$, dominant correlation effects are still determined or at least influenced by the Hamiltonians (23), (15), and (21) with properly renormalized parameters. Examples are the magnetic structure factor (Sec. IV A), the specific heat (Sec. IV C 2) and the degenerate superconducting saddle-point discussed in Ref. 45. An account of the temperature dependence of the corrections due to the hybridization terms $t_{i,h,\perp,z}$ is given at the beginning of Sec. IV.

(iii) As discussed in Ref. 45 the interplane hopping is the important parameter for the mean-field superconducting transition and is estimated to be $t_\perp \sim 20$ meV. The resulting coefficient $t_\perp^2/v_F \sim 6$ K of the interplane pair hopping term is consistent with the transition temperature of $T_c = 1.5$ K on the mean-field level.

IV. APPLICATION TO Sr_2RuO_4

The model derived in Sec. II readily accounts for the observed normal phase properties in Sr_2RuO_4. The most striking qualitative evidence is the recently discovered scale invariance of the magnetic structure factor[29] in agreement with the implications from the effective one-dimensional model Eq. (23). The scale invariance has been observed for $T = 60, 110, 160$ K while it starts to break down[29] at $T = 10$ K which is in the regime of Fermi liquid behavior.[8,41]

Therefore the hierarchy of the applicability of the model derived in Sec. II can be summarized as follows. For $T > 400$ K we expect crossed sliding Luttinger liquid behavior.[51,62] Curvature corrections to the linearized bands of the order of 10% are conceivable at $T \sim 700$ K. For 400 K $> T >$ 25 K the system gradually crosses over to the Fermi liquid regime because the various coupling terms discussed in Sec. III become relevant at different temperatures.[64] The observed scale invariance of the magnetic excitations suggest that these relevant terms mostly impact the quasi-two-dimensional charge channel given by Eq. (15). The one- to two-dimensional crossover of the magnetic subsystem given by Eq. (16) is determined by $\overline{V}_m$. Since the charge and magnetic channels are coupled via Eq. (21) the Fermi liquid behavior only is fully observed in the electronic channel when the quasi-one-dimensional magnetic fluctuations are frozen out for $T \lesssim \overline{V}_m$. From the experimentally observed onset of Fermi liquid behavior[8,41] we estimate $\overline{V}_m \approx 25$ K. Equivalently, a crossover to non-Fermi liquid behavior on energy scales $\omega > 2$ meV is expected.

A. Incommensurate magnetism

An important probe for the interaction effects in correlated electron systems is the magnetic structure factor determined by neutron scattering. The quasi-one-dimensional model derived in Sec. II B accounts for the dominant features of the magnetic response.

The bosonization approach correctly describes excitations near the Fermi surface,[49] i.e., for momentum transfer $q \sim 0$ and $q \sim 2k_F$. The relevant momentum transfer for antiferromagnetic magnetic excitations[65] is $q \sim 2k_F$ since the integrated intensity of the structure factor for $q \rightarrow 0$ vanishes.[66] A one-dimensional model analogous to that of Eq. (22) with equivalent bosonized Hamiltonian and incommensurate back scattering wave vector $q \neq \pi/a$ is the antiferromagnetic Heisenberg chain in a uniform field.[67] We thus expect the effective one-dimensional Hamiltonian Eq. (22) to describe an excitation spectrum as determined in Ref. 68 and sketched in Fig. 2. Since Eq. (22) is a one-dimensional model along the diagonal of the basal plane of the unit cell of Sr_2RuO_4, since the model is manifestly invariant under the symmetry transformations $x \leftrightarrow y$ and $y \rightarrow -y$, and since wave vectors are only defined modulus a reciprocal lattice vector we find gapless magnetic excitations with linear dispersion at $\boldsymbol{q}_i = (\pm[(2\pi/a) - 2k_F],\ \pm[(2\pi/a) - 2k_F])^\dagger \approx (\pm 0.6\pi/a,\ \pm 0.6\pi/a)$ [compare Fig. 1 and Refs. 33 and 69].

The result from conformal field theory for any two point correlation function[65,48] is valid for sufficiently small frequencies ω and momenta $\overline{q} = (q - |\boldsymbol{q}_i|)a$ measured with respect to the back scattering wave vector.

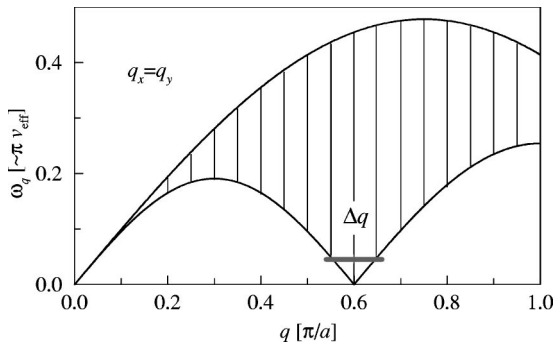

FIG. 2. Sketch of the spectrum of the elementary magnetic excitations of a Heisenberg chain in a magnetic field as adapted from Ref. 68. It models the magnetic excitations of the Hamiltonian Eq. (23) along $q_x=q_y$. The bar marks the width of the spectrum Δq for a given energy transfer.

$$\chi_{\rm m}(\bar{q},\omega)=\frac{A_x}{T^{2-2x}}I_x\left(\frac{\omega-v_{\rm eff}\bar{q}}{2\pi T}\right)I_x\left(\frac{\omega+v_{\rm eff}\bar{q}}{2\pi T}\right), \quad (33)$$

where

$$I_x(k)=\frac{\Gamma(x/2-ik/2)}{\Gamma(1-x/2-ik/2)} \ . \quad (34)$$

The value of the scaling dimension x and the excitation velocity $v_{\rm eff}$ depend on the details of the system. The prefactor A_x depends on the scaling dimension. Please refer to Ref. 70 for details.

The limits of the applicability of the result from conformal field theory can be understood in the framework of studies of Heisenberg chains performed in Ref. 70. It has been shown that the effective scaling dimension x is temperature dependent. At or above temperatures of the order of the excitation velocity, i.e., $T\gtrsim v_{\rm eff}$ we expect the scaling dimension to attain the noninteracting limit, i.e., $x\to 1$. At energy transfers of the order of and above the excitation velocity lattice corrections become relevant. Similar arguments hold for the momentum transfer. At finite temperatures and finite energy transfer the effects combine and the range of validity of Eq. (33) can roughly be estimated as $\sqrt{T^2+\omega^2+(v_{\rm eff}\bar{q})^2}\leqslant v_{\rm eff}/2$.

The following experimental observations can be understood within the framework of the outlined analogies.

(i) The imaginary part of the magnetic correlation function at small energy transfer is strongly peaked at $\boldsymbol{q}_i$ and flat elsewhere.[65,66] This is in perfect qualitative agreement with the magnetic structure factor $S(\boldsymbol{q},\omega)\sim \mathrm{Im}\,\chi_{\rm m}(\boldsymbol{q},\omega)$ determined via inelastic neutron scattering.[28,29]

(ii) The magnetic correlation function Eq. (33) is scale invariant. The scale invariance has been observed experimentally outside the Fermi liquid regime[29] and suggests values of $1/2\leqslant x\leqslant 5/8$ for Sr_2RuO_4. Note that these values of x describe a XXZ Heisenberg chain near the isotropic point,[71] i.e., $J\gtrsim J_z$ for in-plane (J) and out-of-plane (J_z) magnetic coupling,[70] and are thus in quantitative agreement with the intermediate coupling regime assumed for Sr_2RuO_4 within this approach.

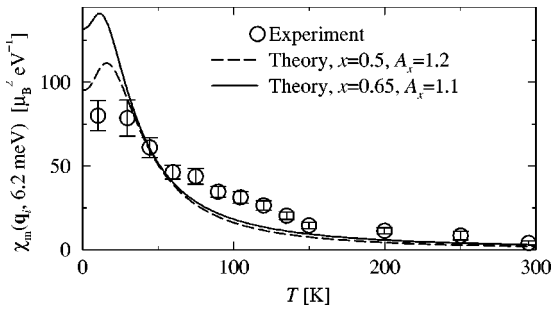

FIG. 3. Plot of $\chi_{\rm m}(0,6.2\ \mathrm{meV})$ from Eq. (33) for $x=0.5$ (broken line) and $x=0.65$ (full line) in comparison with experimental[28] results. Good agreement of the fits for fixed x can only be expected in the temperature interval $2\bar{V}_{\rm m}\leqslant T\ll v_{\rm eff}$.

(iii) Figure 3 shows the temperature dependence of $\mathrm{Im}\,\chi_{\rm m}(0,6.2\ \mathrm{meV})$ from Eq. (33) for $x=0.5$ (broken line) and $x=0.65$ (full line) in comparison with experimental[28] results. The fits are only valid outside the Fermi liquid regime, i.e., for $T>25$ K. Together with the limitations of the applicability of Eq. (33) discussed above the agreement of the fits for fixed x with the experimental data can only be expected in a small temperature interval of $2\bar{V}_{\rm m}\leqslant T\ll v_{\rm eff}$. Note the relatively large energy transfer of $\omega=6.2$ meV $=73$ K. Consequently a discrimination between $x=0.5$ and $x=0.65$ is not conclusive. The prefactors $A_{0.5}=1.2$ and $A_{0.65}=1.1$ are of the correct order of magnitude. Neutron scattering results at lower energy transfer are desirable.

(iv) The experimental results show a width of the magnetic peaks which is only weakly temperature dependent[28] as shown by the circles in Fig. 4. In the model presented here the finite width of the dynamic magnetic correlations follows out of the dispersion of the lower bounds of the excitation continuum as indicated by the bar near $q\sim(2\pi/a)-2k_{\rm F}$ in Fig. 2 with $\Delta q\sim(2\omega/v_{\rm eff}a)$.

The temperature dependence of the excitation velocity can be estimated by considering the magnetic correlation function $\mathrm{Im}\,\chi_{\rm m}(\bar{q},6.2\ \mathrm{meV})$ from Eq. (33) as a function of $\bar{q}$ and determining the full width at half maximum. The results are shown for $x=0.5$ and $v_{\rm eff}=350$ K as the squares in Fig. 4. Consistent with the expected limits of validity of Eq. (33) and the temperature dependence of the peak intensity discussed in paragraph (iii) the values of Δq are in good agree-

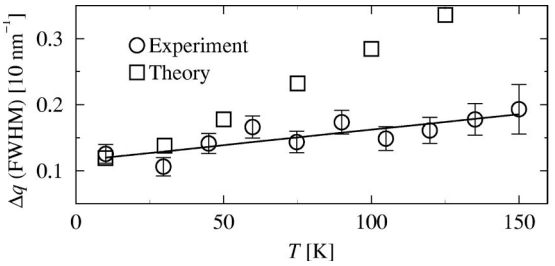

FIG. 4. Full width at half maximum as determined by neutron scattering[28] (circles) and as obtained from Eq. (33) with $\omega=6.2$ meV, $x=0.5$, and $v_{\rm eff}=350$ K (squares). The theoretical values for $T\geqslant 75$ K are less reliable since T and $\bar{q}$ become too large. The line is a guide to the eye.

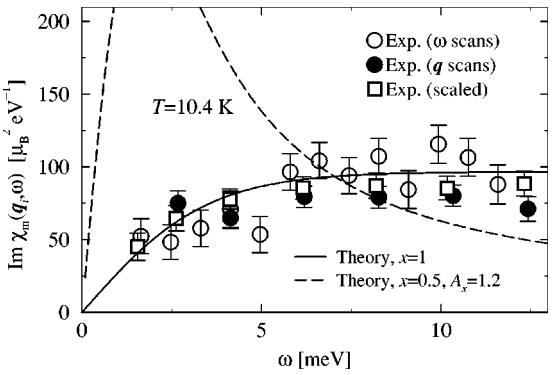

FIG. 5. Plot of $\mathrm{Im}\,\chi_{\mathrm{m}}(0,\omega)|_{T=10.4\ \mathrm{K}}$ from Eq. (33) for $x=1$ (full line) and $x=0.65$ (broken line) in comparison with experimental results for frequency scans (open circles[28] and open squares[29]) and momentum scans (full circles[28]). Since at $T\sim 10$ K the system is in the Fermi liquid regime and for $\omega>2$ meV only gradually crosses over to the conformally invariant regime the applicability of Eq. (33) is not obvious (see text).

ment with the experimental data only for $T<75$ K. Note that for $T>75$ K also the relevant values of $\overline{q}$ become large. For $x=0.65$ the results only differ of the order of 10% and do not allow for any quantitative discrimination. We conclude that the magnetic energy scale is given by $v_{\mathrm{eff}}\sim 10^2$ K.[72]

(v) The symbols in Fig. 5 show the energy dependence of $\mathrm{Im}\,\chi_{\mathrm{m}}(0,\omega)$ at $T=10.4$ K from neutron scattering measurements. Open and full circles are from Ref. 28 for energy and $\boldsymbol{q}$ scans, respectively. Squares from Ref. 29 are scaled since no absolute scale is given. The data are in qualitative agreement with the presence of an excitation continuum.

Since for $T=10.4$ K the system is in the Fermi liquid regime the applicability of Eq. (33) is not obvious. The experimental data can be fitted with the (renormalized) noninteracting case, where[71] $x=1$ and $\mathrm{Im}\,\chi_{\mathrm{m}}(0,\omega)\sim v_{\mathrm{eff}}^{-1}\tanh[\omega/(4T)]$ as shown by the full line in Fig. 5. The amplitude of the fit has been chosen as $v_{\mathrm{eff}}=120$ K consistent with $v_{\mathrm{eff}}\sim 10^2$ K. The good agreement of the fit is likely to be accidental since for larger frequencies $\omega>2$ meV the system should gradually cross over from Fermi liquid to conformal behavior. For $\omega\sim v_{\mathrm{eff}}$ effects from the upper continuum limit become relevant[70] voiding the direct applicability of Eq. (33) for $\omega\gtrsim 10$ meV. Since the details of the crossover are not known, a direct comparison with the results from conformal field theory is not possible. The broken line in Fig. 5 shows the result for the interacting case with $x=0.5$ and $A_{0.5}=1.2$ as determined under (iii) for completeness.

Measurements of the low-energy dynamical structure factor outside the Fermi liquid regime at $30\ \mathrm{K}\leqslant T\leqslant 50$ K are desirable to test the theory presented here in its range of applicability and allow conclusive comparison with perturbative[36] results.

(vi) The presence of quasi-one-dimensional correlations along the system diagonals finds further experimental support in the nonanalytic angular dependence of the in-plane upper critical fields.[46]

In conclusion the functional dependence of the dominant magnetic correlations anticipated from conformal field theory as given by Eq. (33) describes the experimental data satisfactorily within the framework of the expected applicability of the theory. The consistency of the results suggests that we were able to extract a reliable energy scale for the effective magnetic correlations.

B. Comparison with RPA

The magnetic correlations in Sr_2RuO_4 have been widely studied theoretically[26,29,35–38,42,73] using perturbative approaches such as the random-phase-approximation (RPA). The perturbative approaches cannot account for the low-dimensional quantum fluctuations and it is instructive to discuss the resulting limits of their applicability. To this end we have performed a RPA analysis of the magnetic structure factor. The interaction is included in the dynamical correlation functions via[74]

$$\chi^{\nu,\nu'}_{\mathrm{RPA}}(\boldsymbol{q},\omega)=\chi^{\nu,\nu'}_{0}(\boldsymbol{q},\omega)[1-U^{\nu,\nu'}_{\sigma,\sigma'}\chi^{\nu,\nu'}_{0}(\boldsymbol{q},\omega)]^{-1}. \tag{35}$$

The bare susceptibilities $\chi^{\nu,\nu'}_{0}(\boldsymbol{q},\omega)$ are the Fourier transforms of the real time spin-spin correlation function $-i\,\theta\langle \boldsymbol{S}^{\nu}_{\boldsymbol{q}}(t)\boldsymbol{S}^{\nu'}_{-\boldsymbol{q}}(0)\rangle$ and are determined with respect to the tight-binding model discussed in Sec. III. The spin operators $\boldsymbol{S}^{\nu}_{\boldsymbol{q}}(t)$ act on electrons with orbital index $\nu,\nu'\in\{x,y,\gamma\}$. In the absence of Hund's rule coupling the interactions are $U^{\nu=\nu'}_{\sigma\neq\sigma'}=U_0$ and $U^{\nu\neq\nu'}_{\sigma,\sigma'}=U_1=U_2$. For $U_1\neq U_2$ the correlation function contributions to $\chi^{\nu,\nu'}_{\sigma,\sigma'}$ are also anisotropic in the spin Hilbert space.[59] A very recent approach[73] including Hund's rule coupling suggests the stabilization of a chiral magnetic state. The thermodynamic expectation values are determined via the interaction free Hamiltonian with tight-binding bands as shown in Fig. 1 and given in Eqs. (31) and (32).

Figure 6 shows $\mathrm{Im}\,\chi^{\mathrm{tot}}_{\mathrm{RPA}}(\boldsymbol{q},\omega)=\mathrm{Tr}\,\mathrm{Im}\,\chi^{\nu,\nu'}_{\mathrm{RPA}}(\boldsymbol{q},\omega)$ for $\omega=6.2$ meV convoluted with the resolution $\delta q\approx 0.1\pi/a$ from neutron scattering experiments[28] (a) for $k_z=0$ and (b) for $k_z=\pi/c$. The interaction parameters here are $U_0=0.2$ eV, $U_1=0.1$ eV, and $U^{x,\gamma}_{\sigma,\sigma'}=U^{y,\gamma}_{\sigma,\sigma'}=0$. This neglects the hybridization of the d_{xy} band with the d_{zx} and d_{yz} bands which has a quantitative effect on $\chi^{\gamma,\gamma}_{\mathrm{RPA}}(\boldsymbol{q},\omega)$,[36] but not so much on the total correlation function. The features discussed in Ref. 36 are reproduced albeit with different weight.

Panel (a) of Fig. 6 shows the correlations in the plane through the Γ point of the Brillouin zone ($k_z=0$) while the correlations in (b) lie in the plane through the midpoint of the line $\overline{\Gamma Z}$ ($k_z=\pi/c$).[24] The difference of the two shows the sensitivity of the RPA approach to small changes in the parameters.

The total correlation function in RPA in Fig. 6 clearly shows the structures of the bands dispersing in the plane. Many of these structures have not been observed experimentally.[29] Moreover, the parameters have to be fine tuned in the RPA approach close to a phase transition.[28] Both effects can be understood as consequences of the underestimation of quantum fluctuations.

Quantum fluctuations in low-dimensions suppress long-range order even if the value of the interaction is large

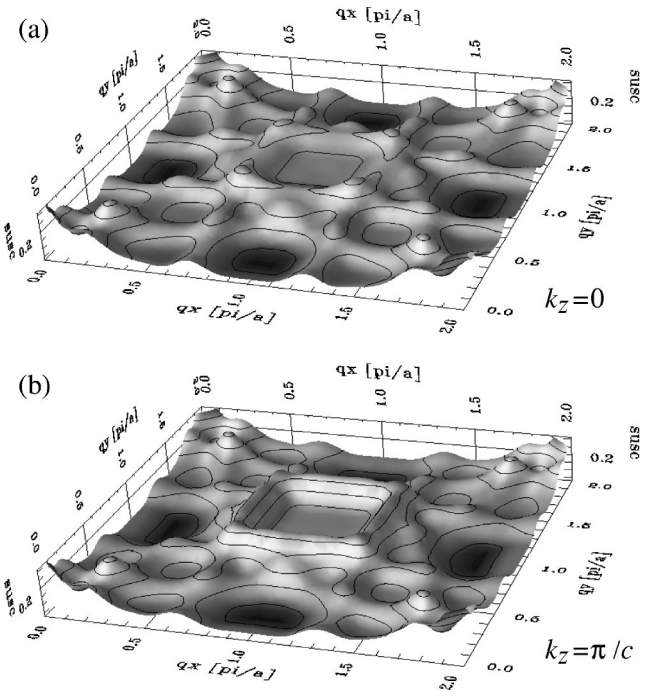

FIG. 6. Tr Im $\chi^{\nu,\nu'}_{\mathrm{RPA}}(\boldsymbol{q},\omega)$ convoluted with the experimental q resolution. Parameters are $\omega=6.2$ meV, $U_0=0.2$ eV, $U_1=0.1$ eV, $U^{x,\gamma}_{\sigma,\sigma'}=U^{y,\gamma}_{\sigma,\sigma'}=0$ and dispersions Eqs. (31) and (32). Panel (a) $k_z=0$ and (b) $k_z=\pi/c$ show the sensitivity of the RPA approach to small changes in the parameters.

enough to give a finite temperature phase transition in RPA.[75] More specifically, for the one-dimensional case—which is discussed closely in the review by Sólyom[76]—the relevance of back and umklapp scattering terms is overestimated by perturbative approaches such as RPA. Instead, their relevance has to be determined nonperturbatively, namely, via renormalization group (RG) studies.

Consequently the two-dimensional RPA approach tends to underestimate the one-dimensional correlations since the renormalization of the excitation velocities can only be modeled indirectly by the interaction strength while the relative size of the two-dimensional features tends to be overestimated. Because of the large parameter space of the RPA approach and the sensitivity to details in the band structure it is still possible to model the low-temperature magnetic structure factor in Sr_2RuO_4 rather accurately.[29] The weakness of the RPA approach becomes apparent through the fact that the description of different properties of the material requires different choices of parameter sets.[36,38]

The present approach allows to include the RG results from the literature[43] since the back and umklapp scattering terms are given explicitly by Eq. (21) as discussed in Sec. II A. The quantum fluctuations and interaction effects are included by the renormalization of parameters such as v_{eff} and their impact becomes apparent through the small scaling dimension x discussed in Sec. IV A.

In conclusion the incommensurate magnetic fluctuations in Sr_2RuO_4 are best described via the quasi-one-dimensional correlations from Eq. (23) with a spectrum as sketched in Fig. 2.[69] The two-dimensional correlations yield an enhanced but relatively homogeneous background with only small additional structures.[29] Note that the two-dimensional magnetic correlations beyond the diagonals are given within the present approach by Eq. (16).

C. Effective electronic masses

In the following we will discuss effective electronic masses observed in the Fermi liquid regime of Sr_2RuO_4. Clearly, a system that shows scale invariant correlations down to 25 K must show a different renormalization of the Fermi liquid parameters than a system that is a Fermi liquid at all temperatures. Consequently it is quite natural to estimate that difference phenomenologically by considering that there is a very strong reduction of the effective excitation velocity of $v_{\mathrm{F}}/v_{\mathrm{eff}}\sim 20$–$60$ in the magnetic sector along the diagonals of the basal plane due to interaction effects as discussed in Sec. IV A. In the Fermi liquid regime this reduction cannot be calculated directly via the results from conformal field theory (Sec. IV A) because of the two-dimensional coupling $\overline{V}_{\mathrm{m}}$ (Sec. II A). It is yet reasonable to assume that the reduction of the excitation velocity in the magnetic channel along the diagonals remains much larger than the mere factor of 2 (see below) obtained in perturbative[35] approaches. With this assumption the different electronic masses can be modeled.

1. Cyclotron mass

The cyclotron mass m_{c} determines the cyclotron frequency and has been measured in dHvA experiments[41,42] to be enhanced with respect to the bare (noninteracting) band mass m_{b} on all three Fermi surfaces by the same amount, namely, $m_{\mathrm{c}}^{(\alpha,\beta,\gamma)}/m_{\mathrm{b}}^{(\alpha,\beta,\gamma)}\approx 2$. Since the cyclotron motion does not involve magnetic excitations the cyclotron mass enhancement due to interactions is determined in the present approach by the quasi-two-dimensional Hamiltonian of the charge channel Eq. (15) in the subsystem of the d_{zx} and d_{yz} electrons. Perturbative approaches with an appropriate choice of parameters[35] also yield an electronic mass enhancement factor of 2 for all bands. ARPES measurements are consistent with this result.[7,24]

2. Specific heat

The specific heat of an interacting system can be determined from the specific heat of the noninteracting system via the renormalization of the thermodynamic mass[42] m^* with respect to the bare band mass m_{b} or, equivalently, by the renormalized excitation velocities[43] v_{F}^* or v_{eff} with respect to the bare band Fermi velocity v_{F}.

The specific heat of the d_{zx}-d_{yz} subsystem C_z consists of the two-dimensional contributions from the spin and charge channels [Eqs. (15) and (16)] and the ''one-dimensional'' magnetic part along the diagonals [Sec. IV B]. The renormalized velocity of the two-dimensional contributions is given through the cyclotron mass enhancement as $v_{\mathrm{F}}/v^*_{\mathrm{F,2D}}\approx 2$. The quasi-one-dimensional magnetic correlations with excitation velocity v_{eff} are only present along the diagonals of the Brillouin zone. Consequently their contribution to the total

specific heat must be weighed with respect to a system with one-dimensional magnetic correlations throughout the entire Brillouin zone. The normalized width of the magnetic peaks $(a/2\pi)\Delta q \sim 0.07$ discussed in Sec. IV A allow for an estimate. Depending on whether one assumes quasi-one-dimensional correlations in the vicinity of the positions of the incommensurate fluctuations $\boldsymbol{q}_i$ only or along the whole diagonals weighing factors of $0.02 \leqslant w \leqslant 0.2$ are reasonable. The weight of the two-dimensional magnetic contribution then is $1-w$.

Together the contributions yield the specific heat of the d_{zx}-d_{yz} subsystem as[43]

$$\frac{C_z}{T} = \gamma_z \gamma_0 \approx \frac{v_F}{2}\left(\frac{1}{v^*_{F,2D}} + \frac{1-w}{v^*_{F,2D}} + \frac{w}{v_{eff}}\right)\gamma_0 . \qquad (36)$$

The value of $\gamma_z \approx (m^*_\alpha/m_b^{(\alpha)} + 2m^*_\beta/m_b^{(\beta)})/3 \approx 3.4$ can be estimated from a weighed average of the thermodynamic masses $m^*_\alpha/m_b^{(\alpha)} \approx 3.1$ and $m^*_\beta/m_b^{(\beta)} \approx 3.5$ measured via the dHvA effect.[42] Then the ''one-dimensional'' magnetic contribution is determined as $w\, v_F/2\, v_{eff} \approx 1.4 + w$. Using the value of $v_{eff} = 350$ K considered in Sec. IV A (iv) and the bare Fermi velocity[27] $v_F \approx 0.7$ eV then gives $w = 0.13$.

It must be pointed out that the two-dimensional coupling $\sim \overline{V}_m \ll V_m$ is likely to increase the effective velocity v_{eff} in the Fermi liquid regime through the reduction of the correlation effects. This increase is compensated by an increase of the relevant phase space in the Brillouin zone determined by w. The phenomenological result that the strong low-dimensional magnetic correlations with $v_{eff} \ll v^*_{F,2D}$ enhance the specific heat beyond the value obtained via perturbative approaches[35] remains unaltered.

For noninteracting electrons in the two quasi-one-dimensional bands under consideration the coefficient $\gamma_0 \approx 4.3$ mJ/K^{2}mol results in a specific heat contribution of $C_z/T \approx 15$ mJ/K^2 mol that accounts for about 40% of the experimentally observed value of $\gamma_{tot} = 40 \pm 2$ mJ/K^2 mol.[30–32,42]

Hydrostatic pressure increases the in-plane single-particle hopping which decreases the relative interaction strength and renders the d_{zx}-d_{yz} subsystem more two dimensional. Consequently the ''one-dimensional'' magnetic contribution in Eq. (36) is decreased yielding a natural explication for the observed reduction of the thermodynamic masses upon application of hydrostatic pressure[42] within the present model.

The thermodynamic mass of the d_{xy} electrons is enhanced by a factor of $m^*_\gamma/m_b^{(\gamma)} \sim 5.5$ with respect to the bare band mass.[42] The renormalized Fermi velocity from ARPES[7,24] or perturbative approaches[35] only accounts for a factor of 2. The interaction between the d_{xy} band and the d_{zx}-d_{yz} system accounts for a part of the missing enhancement through coupling to the one-dimensional correlations in the magnetic channel. Another possible contribution comes from the proximity of the d_{xy} band to the van Hove singularity at the M point of the Brillouin zone.[35] Nesting effects[36,37] yield an additional enhanced magnetic contribution to the specific heat.

3. Static susceptibility and Wilson ratio

Following the argumentation of the specific heat the contributions to the uniform static magnetic susceptibility of the d_{zx}-d_{yz} subsystem also consist of a two- and one-dimensional part. They are given with respect to the static magnetic susceptibility of the noninteracting system χ_0 as[43]

$$\chi_z \approx \chi_0\left(\frac{v_F(1-w)}{v^*_{F,2D}} + \frac{w\, v_F}{v_{eff}}\right) \approx 4.3\chi_0 . \qquad (37)$$

All parameters have been fixed previously. Note that here the relative contribution of the ''one-dimensional'' subsystem is roughly twice that of the specific heat since γ_0 includes both magnetic and charge degrees of freedom while χ_0 only accounts for the magnetic correlations.

The enhancement of the susceptibility is in reasonable agreement with the relative spin-mass enhancement of the α and β sheets measured via the dHvA effect[41,42] as $m^*_{\alpha,susc}/m_b^{(\alpha)} \approx 3.7$ and $m^*_{\beta,susc}/m_b^{(\beta)} \approx 4.3$. Moreover, since the model derived in Sec. II A predicts the quasi-one-dimensional magnetic correlations only in the basal plane of the tetragonal lattice we expect a magnetic mass enhancement that depends on the position k_z on the Fermi surface with maxima at $k_{z,max}(n) = 2\pi n/c$ as observed[42] experimentally.

The ratio of the uniform static magnetic susceptibility and the specific heat coefficient has been determined experimentally as $R_W = (\pi^2\chi)/(3\gamma_{tot}) \approx 1.4$.[8,13] The value of $R_{W,z} \approx 1.3$ obtained here for the d_{zx}-d_{yz} subsystem is in good agreement. The enhancement of the specific heat has indeed the same origin as the enhancement of the susceptibility as already concluded in Ref. 1 which can be identified in the d_{zx}-d_{yz} subsystem as the quasi-one-dimensional magnetic correlations.

An interesting experimental question that arises out of the discussion above is whether the photoelectrons carry signatures of the enhanced magnetic correlations along the diagonals. To obtain an answer ARPES data for the α and β sheets need to be analyzed in detail along $\overline{\Gamma X}$ in comparison with $\overline{\Gamma M}$ and $\overline{MX}$. Using the value extracted in Sec. IV A (iv) the expected energy scale is $v_{eff} \sim 30$ meV.

V. CONCLUSIONS

The dominantly one-dimensional kinetic energy of the electrons in the d_{zx} and d_{yz} orbitals allows to bosonize their Hamiltonian. In the presence of interaction this leads to an effective two-dimensional model. The degrees of freedom can be parametrized in terms of the four spin, charge, flavor, and spin-flavor fields.

The presence of hybridization and corrections to the one-dimensional kinetic energy make the observation of properties of sliding Luttinger liquids likely only at or above room temperature. This is consistent with the observed linear temperature dependence of the resistivity at high temperatures.

In the magnetic sector described by the spin and spin-flavor fields the interaction at intermediate coupling leads to a quasi-one-dimensional model along the diagonals of the

basal plane of the Brillouin zone. The resulting spectrum of elementary excitations accounts for the enhanced dynamical magnetic susceptibility at $\boldsymbol{q}_i=(\pm 2k_F, \pm 2k_F)$ and the weak temperature dependence of the q width. The one-dimensional spectrum leads to a conformally invariant formulation of the magnetic structure factor consistent with the observed scale invariance. The scaling dimension is consistent with the intermediate coupling regime. The observed excitation continuum and temperature dependence of the peak width are consistent with a magnetic energy scale of $v_{\mathrm{eff}} \sim 10^2$ K. The additional two-dimensional correlations are more homogeneous than predicted by RPA because of quantum fluctuations.

The effective thermodynamic mass enhancement together with the value of the specific heat coefficient is a superposition of two-dimensional effects as observed in ARPES and the ''quasi-one-dimensional'' correlations of the magnetic channel of the d_{zx}-d_{yz} subsystem. The enhancement of the static susceptibility has the same origin. The contribution of the quasi-one-dimensional magnetic subsystem to the specific heat of the d_{zx}-d_{yz} subsystem is about 44% and about 70% to the static magnetic susceptibility of the d_{zx}-d_{yz} subsystem.

ACKNOWLEDGMENTS

We are thankful to C. Bergemann, M. Braden, S. T. Carr, N. Dietz, K. Kikoin, M. S. Laad, S. Sachdev, G. Schneider, A. M. Tsvelik, T. Valla, W. Weber, and M. Weinert for instructive and stimulating discussions. The work was supported by DOE Contract No. DE-AC02-98CH10886.

*Present address: Institut für Theorie der Kondensierten Materie, Universität Karlsruhe, 76128 Karlsruhe, Germany.

†Deceased.

[1] Y. Maeno, H. Hashimoto, K. Yoshida, S. Nishizaki, T. Fujita, J.G. Bednorz, and F. Lichtenberg, Nature (London) **372**, 532 (1994).

[2] M. Braden, W. Reichardt, S. Nishizaki, Y. Mori, and Y. Maeno, Phys. Rev. B **57**, 1236 (1998).

[3] A.P. Mackenzie, S.R. Julian, A.J. Diver, G.J. McMullan, M.P. Ray, G.G. Lonzarich, Y. Maeno, S. Nishizaki, and T. Fujita, Phys. Rev. Lett. **76**, 3786 (1996).

[4] T. Oguchi, Phys. Rev. B **51**, 1385 (1995).

[5] M. Schmidt, T.R. Cummins, M. Bürk, D.H. Lu, N. Nücker, S. Schuppler, and F. Lichtenberg, Phys. Rev. B **53**, R14 761 (1996).

[6] Y. Maeno, T.M. Rice, and M. Sigrist, Phys. Today **54** (1), 42 (2001).

[7] A.V. Puchkov, Z.-X. Shen, T. Kimura, and Y. Tokura, Phys. Rev. B **58**, R13 322 (1998).

[8] Y. Maeno, K. Yoshida, H. Hashimoto, S. Nishizaki, S. Ikeda, M. Nohara, T. Fujita, A.P. Mackenzie, N.E. Hussey, J.G. Bednorz, and F. Lichtenberg, J. Phys. Soc. Jpn. **66**, 1405 (1997).

[9] A.P. Mackenzie, S. Ikeda, Y. Maeno, T. Fujita, S.R. Julian, and G.G. Lonzarich, J. Phys. Soc. Jpn. **67**, 385 (1998).

[10] K. Ishida, H. Mukuda, Y. Kitaoka, Z.Q. Mao, Y. Mori, and Y. Maeno, Phys. Rev. Lett. **84**, 5387 (2000).

[11] R.J. Cava, B. Batlogg, K. Kiyono, H. Takagi, J.J. Krajewski, W.F. Peck, L.W. Rupp, and C.H. Chen, Phys. Rev. B **49**, 11 890 (1994).

[12] T.M. Rice and M. Sigrist, J. Phys.: Condens. Matter **7**, L643 (1995).

[13] K. Ishida, Y. Kitaoka, K. Asayama, S. Ikeda, S. Nishizaki, Y. Maeno, K. Yoshida, and T. Fujita, Phys. Rev. B **56**, R505 (1997).

[14] K. Ishida, H. Mukuda, Y. Kitaoka, K. Asayama, Z.Q. Mao, Y. Mori, and Y. Maeno, Nature (London) **396**, 658 (1998).

[15] J.A. Duffy, S.M. Hayden, Y. Maeno, Z. Mao, J. Kulda, and G.J. McIntyre, Phys. Rev. Lett. **85**, 5412 (2000).

[16] G.M. Luke, Y. Fudamoto, K.M. Kojima, M.I. Larkin, J. Merrin, B. Nachumi, Y.J. Uemura, Y. Maeno, Z.Q. Mao, Y. Mori, H. Nakamura, and M. Sigrist, Nature (London) **394**, 558 (1998).

[17] G. Baskaran, Physica B **223-224**, 490 (1996).

[18] F. Laube, G. Goll, H.v. Löhneysen, M. Fogelström, and F. Lichtenberg, Phys. Rev. Lett. **84**, 1595 (2000).

[19] Z.Q. Mao, K.D. Nelson, R. Jin, Y. Liu, and Y. Maeno, Phys. Rev. Lett. **87**, 037003 (2001).

[20] M.A. Tanatar, S. Nagai, Z.Q. Mao, Y. Maeno, and T. Ishiguro, Phys. Rev. B **63**, 064505 (2001).

[21] M.A. Tanatar, M. Suzuki, S. Nagai, Z.Q. Mao, Y. Maeno, and T. Ishiguro, Phys. Rev. Lett. **86**, 2649 (2001).

[22] K. Izawa, H. Takahashi, H. Yamaguchi, Y. Matsuda, M. Suzuki, T. Sasaki, T. Fukase, Y. Yoshia, R. Settai, and Y. Onuki, Phys. Rev. Lett. **86**, 2653 (2001).

[23] H. Yaguchi, T. Akima, Z.Q. Mao, Y. Maeno, and T. Ishiguro, Phys. Rev. B **66**, 214514 (2002).

[24] A. Damascelli, D.H. Lu, K.M. Shen, N.P. Armitage, F. Ronning, D.L. Feng, C. Kim, Z.-X. Shen, T. Kimura, Y. Tokura, Z.Q. Mao, and Y. Maeno, Phys. Rev. Lett. **85**, 5194 (2000).

[25] K.M. Shen, A. Damascelli, D.H. Lu, N.P. Armitage, F. Ronning, D.L. Feng, C. Kim, Z.-X. Shen, D.J. Singh, I.I. Mazin, S. Nakatsuji, Z.Q. Mao, Y. Maeno, T. Kimura, and Y. Tokura, Phys. Rev. B **64**, 180502(R) (2001).

[26] I.I. Mazin and D.J. Singh, Phys. Rev. Lett. **82**, 4324 (1999).

[27] I.I. Mazin, D.A. Papaconstantopoulos, and D.J. Singh, Phys. Rev. B **61**, 5223 (2000).

[28] Y. Sidis, M. Braden, P. Bourges, B. Hennion, S. NishiZaki, Y. Maeno, and Y. Mori, Phys. Rev. Lett. **83**, 3320 (1999).

[29] M. Braden, Y. Sidis, P. Bourges, P. Pfeuty, J. Kulda, Z. Mao, and Y. Maeno, Phys. Rev. B **66**, 064522 (2002).

[30] S. Nishizaki, Y. Maeno, and S. Farner, J. Phys. Soc. Jpn. **67**, 560 (1998).

[31] S. Nishizaki, Y. Maeno, and Z.Q. Mao, J. Low Temp. Phys. **117**, 1581 (1999).

[32] S. Nishizaki, Y. Maeno, and Z.Q. Mao, J. Phys. Soc. Jpn. **69**, 572 (2000).

[33] I.I. Mazin and D. Singh, Phys. Rev. Lett. **79**, 733 (1997).

[34] G. Litak, J.F. Annett, and B.L. Györffy, in *Superconductivity in Disordered* Sr_2RuO_4, edited by S. Sarkar (Kluwer Academic Publishers, Dordrecht, 2000), pp. 307–316; cond-mat/0012099.

[35] A. Liebsch and A. Lichtenstein, Phys. Rev. Lett. **84**, 1591 (2000).

[36] I. Eremin, D. Manske, C. Joas, and K.H. Bennemann, Europhys. Lett. **58**, 871 (2002).

[37] I. Eremin, D. Manske, and K.H. Bennemann, Phys. Rev. B **65**, 220502 (2002).

[38] D.K. Morr, P.F. Trautman, and M.J. Graf, Phys. Rev. Lett. **86**, 5978 (2001).
[39] K. Kuroki, M. Ogata, R. Arita, and H. Aoki, Phys. Rev. B **63**, 060506(R) (2001).
[40] J.F. Annett, G. Litak, B.L. Györffy, and K.I. Wysokiǹski, Phys. Rev. B **66**, 134514 (2002).
[41] C. Bergemann, S.R. Julian, A.P. Mackenzie, S. NishiZaki, and Y. Maeno, Phys. Rev. Lett. **84**, 2662 (2000).
[42] C. Bergemann, A.P. Mackenzie, S.R. Julian, D. Forsythe, and E. Ohmichi, Adv. Phys. (to be published).
[43] H.J. Schulz, G. Cuniberti, and P. Pieri, cond-mat/9807366 (unpublished), Lecture Notes (Summer school in Chia Laguna, Italy, 1997).
[44] H.J. Schulz, in *The Hubbard Model: Its Physics and Mathematical Physics*, edited by D. Baerisvyl (Plemun, New York, 1995), p. 89; H.J. Schulz, cond-mat/9402103 (unpublished).
[45] R. Werner, following paper, Phys. Rev. B **67**, 014505 (2003).
[46] R. Werner, this issue, Phys. Rev. B **67**, 014506 (2003).
[47] V.J. Emery and S. Kivelson, Phys. Rev. B **46**, 10 812 (1992).
[48] A.O. Gogolin, A.A. Nersesyan, and A.M. Tsvelik, *Bosonization and Strongly Correlated Systems* (Cambridge University Press, Cambridge, 1998).
[49] E.F. Fradkin, *Field Theories of Condensed Matter Systems* (Addison-Wesley, New York, 1991).
[50] D. Sénéchal, cond-mat/9908262 (unpublished).
[51] R. Mukhopadhyay, C.L. Kane, and T.C. Lubensky, Phys. Rev. B **64**, 045120 (2001).
[52] K. Kikoin, I. Kuzmenko, S. Gredeskul, and Y. Avishai, cond-mat/0205120 (unpublished).
[53] I.E. Dzyaloshinskii and A.I. Larkin, Zh. Eksp. Teor. Fiz. **61**, 791 (1971) [Sov. Phys. JETP **34**, 422 (1972)].
[54] V.J. Emery, in *Highly Conducting One-dimensional Solids*, edited by J.T. Devreese, R.P. Evrard, and V. E. van Doren (Plemun, New York, 1979), p. 247.
[55] V.J. Emery, E. Fradkin, S.A. Kivelson, and T.C. Lubensky, Phys. Rev. Lett. **85**, 2160 (2000).
[56] At this point it should be stressed that the tetragonal structure of Sr_2RuO_4 has been found to be very stable (cf. Ref. 2). It is thus admissible to employ the symmetry relations that follow from the tetragonal point group at all temperatures.
[57] From Heisenberg chains it is known that the exact renomalization of the exitation velocity [J. des Cloizeaux and J.J. Pearson, Phys. Rev. **128**, 2131 (1962)] is not correctly reproduced by the bosonization approach [A. Luther and I. Peschel, Phys. Rev. B **12**, 3908 (1975)].
[58] F. Herman and S. Skillman, *Atomic Structure Calculations* (Prentice-Hall, Englewood Cliffs, N.J., 1963).
[59] K.-K. Ng and M. Sigrist, J. Phys. Soc. Jpn. **69**, 3764 (2000).
[60] A. Zheludev, S. Maslov, I. Tsukada, I. Zaliznyak, L.P. Regnault, T. Masuda, K. Uchinokura, R. Erwin, and G. Shirane, Phys. Rev. Lett. **81**, 5410 (1998).
[61] K. Hamacher, C. Gros, and W. Wenzel, Phys. Rev. Lett. **88**, 217203 (2002).
[62] A.W. Tyler, A.P. Mackenzie, S. NishiZaki, and Y. Maeno, Phys. Rev. B **58**, R10 107 (1998).
[63] S.-C. Wang, H.-B. Yang, A. Kaminski, T. Sato, T. Takahashi, Y. Maeno, J. Engelbrecht, X. Dai, Z. Wang, and H. Ding, cond-mat/0204036 (unpublished).
[64] T. Valla, P.D. Johnson, Z. Yusof, B. Wells, Q. Li, S.M. Loureiro, R.J. Cava, M. Mikami, Y. Mori, M. Yoshimura, and T. Sasaki, Nature (London) **417**, 627 (2002).
[65] H.J. Schulz, Phys. Rev. B **34**, 6372 (1986).
[66] M. Karbach, G. Müller, A.H. Bougourzi, A. Fledderjohann, and K.-H. Mütter, Phys. Rev. B **55**, 12 510 (1997).
[67] A. Fledderjohann, C. Gerhardt, K.-H. Mütter, A. Schmitt, and M. Karbach, Phys. Rev. B **54**, 7168 (1996).
[68] M. Karbach and G. Müller, Phys. Rev. B **62**, 14 871 (2000).
[69] R. Werner, cond-mat/0201293 (unpublished).
[70] R. Werner and A. Klümper, Phys. Rev. B **64**, 174414 (2001).
[71] K. Fabricius, U. Löw, and J. Stolze, Phys. Rev. B **55**, 5833 (1997).
[72] The size of the renormalization of $v_{\mathrm{eff}} \sim 10^2$ K with respect to $v_{\mathrm{F}} \sim 10^4$ K is reasonable. The magnetic energy scales in correlated electron systems range from 10 K to 10^3 K while the electronic energy scales are of the order of 1 eV yielding energy ratios of 10 to 10^3.
[73] A.A. Ovchinnikov and M.Y. Ovchinnikova, JETP **95**, 87 (2002).
[74] G.D. Mahan, *Many-particle Physics* (Plemnum Press, New York, 1990).
[75] N.D. Mermin and H. Wagner, Phys. Rev. Lett. **17**, 1133 (1966).
[76] J. Sólyom, Adv. Phys. **28**, 201 (1979).